DEVELOPMENT OF A PREDICTION MODEL FOR SPLASH AND SPRAY

H. VINER, A. DUNFORD, F. COYLE & K. NESNAS
TRL Ltd, Wokingham, United Kingdom
hviner@trl.co.uk
D. HARGREAVES & T. PARRY
University of Nottingham, United Kingdom
david.hargreaves@nottingham.ac.uk
G. FLINTSCH
Virginia Polytechnic Transportation Institute and State University, Virginia
gflintsch@vtti.vt.edu

ABSTRACT

Under some conditions splash and spray create a significant nuisance to road users and some evidence suggests that they contribute to a small but measureable proportion of accidents. This paper reports on the development of a prediction model for splash and spray. The work has been funded by the Federal Highway Administration in order to assist engineers in decisions concerning the type and priority of maintenance on the road network. Ultimately, this could deliver a range of benefits including increased user satisfaction with the network, reduced accidents and a reduction in the detrimental effect of pollutants being deposited on the road verges and street furniture.

The approach taken has been, firstly, to develop a method for predicting the depth of water that builds up on the road surface, considering the rainfall rate, pavement geometry and surface type. Models obtained from the literature have been validated through measurements of water depth carried out in a flume, using a number of typical road surfaces. Secondly, computational fluid dynamics has been used to estimate the level of nuisance to road users of the various mechanisms of splash and spray generation.

1. INTRODUCTION

1.1. Mechanisms and effects of splash/spray generation

The principles of splash and spray generation are broadly accepted: in wet conditions, vehicle tires can cause significant volumes of water to be ejected from the tire/road contact patch. This results in splash – the formation of sizeable, more-or-less intact bodies of water, thought to occur when the void volume within the contact area is insufficient to accommodate the volume of water present on the road. Water is also flung off the tire by the rotation and both sources, when hitting other surfaces, result in the formation of smaller and lighter droplets. These remain in the atmosphere in the form of spray, causing a reduction in visibility to road users.

The effects of splash and spray are further complicated by the turbulent air stream around and behind vehicles, particularly large vehicles travelling at speed. These often cause significant volumes of water to be directed onto the windscreens of other vehicles, resulting in a more drastic and less predictable localized loss of visibility.

Splash and spray are predominantly caused by heavy vehicles [1], with some authors estimating the loss of visibility due to spray arising from a passenger car to be around 1/7 that for a 3-axle lorry. Various attempts have been made to estimate the proportion of

accidents where splash or spray was a contributory factor. Values reported by Tromp [1] ranged from 0.2%, from a Connecticut study, to 4% in a UK study.

A further effect is that fine debris containing a range of pollutants is dislodged from vehicles and the road surface, and deposited on windscreens and headlights - resulting in a more gradual loss of visibility, and on neighbouring verges and street furniture causing environmental and maintenance concerns. As well as leading to splash and spray, the presence of a significant depth of water on the carriageway has other associated problems, such as hydroplaning and excessive reflection of light sources at night, which can obscure lane markings.

1.2. Direct measurement of splash / spray on in-service highways

Numerous attempts have been made to develop equipment for direct measurements on highways. The main configurations are fixed roadside equipment measuring either longitudinally or transversely, relative to the direction of travel, and on-board equipment [2]. Each method has advantages and disadvantages in the accuracy and relevance to drivers; laser transmissometers were found to be the most common type of sensor for measuring spray, and telephotometers and video images are also used.

In Knight's work [2], a video method was developed to assess the feasibility of introducing a spray suppression test within European type approval regulations. The work noted that the technique was not yet suitable for routine application in multiple test facilities by technicians without specialist knowledge as it required careful control of water depth, pavement characteristics, lighting conditions and camera set-up to achieve consistent results. Other challenges, such as control of the camera dynamic range to achieve acceptable luminance under varying conditions, are understood to have been rectified.

A comprehensive review of spray measurement techniques in 2007 [3], concluded that no measurement technique so far identified was suitable for wide scale assessment of pavement performance in relation to splash / spray, due to multiple factors that cannot be standardised or controlled, yet have a substantial impact on the measured results.

1.3. Approach to this work

Since the direct measurement of splash and spray on highways is not yet practical, this work has sought to develop a model for the propensity of pavements to cause nuisance to road users as a result of splash and spray. This has involved, firstly, the development of a model to predict the depth of water on the pavement under different rainfall conditions and, secondly, a model to estimate the creation of splash / spray by commercial vehicles. This paper describes the work undertaken in each of these areas.

2. DEVELOPMENT OF A WATER DEPTH MODEL

2.1. Background

A review of previous research into the build up of water on road surfaces revealed a number of formulae to calculate the depth of water on the pavement. The following five formulae were published with full derivations and have been harmonised here so they have consistent notation and units. The references indicate their source.

$$d = 0.005\, L^{0.5}\, I^{0.5}\, S^{-0.2} \qquad \text{Equation 1} \qquad [4]$$

$$d = 3.38\times10^{-3}\, T^{0.11}\, L^{0.43}\, I^{0.59}\, S^{-0.42} \qquad \text{Equation 2} \qquad [5]$$

$$d = 8.68\times10^{-2}\, T^{0.5}\, L^{0.383}\, I^{0.383}\, S^{-0.333} \qquad \text{Equation 3} \qquad [6]$$

$$d = 3.76 \times 10^{-3} T^{0.125} L^{0.519} I^{0.562} S^{-0.364} \quad \text{Equation 4} \quad [7]$$

$$d = n^{0.6} 36.1^{-0.6} L^{0.6} I^{0.6} S^{-0.3} \quad \text{Equation 5} \quad [7]$$

Where d is the water depth, T is texture depth, L is the length of the flow path (drainage length), I is rainfall rate (intensity), S is slope and n is Manning's coefficient. The units are m or m/hr with the exception of T, which is expressed in mm, and S and n which are dimensionless. It is apparent that these relationships have the general form:

$$d = k T^{w} L^{x} I^{y} S^{z} \quad \text{Equation 6}$$

Where k is a constant that incorporates Manning's coefficient, w is in the range 0.11 to 0.5, x and y are in the range 0.383 to 0.6 and z is in the range -0.42 to -0.2. To establish a water depth model for this project, measurements were carried out in the University of Nottingham flume to calibrate this relationship on pavement surfaces typical of those used in the United States.

2.2. Flume apparatus

The flume apparatus (Figure 1) has a length of 4 m. At the upstream end, water is pumped vertically down into a sump, which overflows into the working section, 0.6 m wide by 0.3 m high. The water is cycled at a rate, Q, measured using rotameters.

Figure 1 - Flume apparatus viewed from the downstream end

Once the flume had reached a steady state, the water depth was measured using wave gauges. These are produced by HR Wallingford and consist of two stainless steel rods of length 300 mm, kept parallel by a plastic head and foot. Wave gauges are simple and reliable devices for measuring water levels; they operate by measuring the current that flows between the two wires which is then converted to an output voltage, directly proportional to the immersed depth. The wave gauges were calibrated for each run by immersing in known depths of still water in the range 0-50 mm. Changes in height could be determined very accurately using a Vernier scale. At low depths, the meniscus made determination of water depth difficult.

2.3. Measurements

Six surfaces (Table 1) were tested in the flume towards its upstream end. The five road surfacing materials were prepared in the laboratory; each consisting of eight, 0.3 m

squares, arranged 4 x 2 down the flume. A Perspex sheet was included to provide a low-textured control surface. Each surface was tested at three slopes by mounting the squares on appropriately angled boards, at 0.5, 2 and 6% slope. Sealant was used to fill the gaps around the mounting board and between the surface squares and this was allowed to set for 24 hours before testing. The experimental campaign therefore consisted of 18 tests, i.e. six surfaces at three angles each.

Table 1 - Surface types and texture depths of the materials tested

Number	Description	Texture depth (mm MPD)
1	Stone Mastic Asphalt	0.55
2	Asphaltic concrete	0.63
3	Smooth concrete	0.21
4	Tined concrete*	1.01
5	Open graded friction course	1.64
6	Perspex	0.001

*Sample orientated with the tined grooves perpendicular to the water flow

Within each test, the flow rate, Q, was varied from 20 l/min to 140 l/min in increments of 20 l/min. The flow rates at the higher end of this range are unrepresentative of surface water on roads but were included to determine whether the trend in the relationship between water depth and flow rate would extrapolate down to the lower flow rates. In all cases it appeared to do so. Water depth relative to the mean level of the surface was determined at the centre of each of the eight road surface squares. This level is difficult to ascertain for the rougher surfaces and presents a source of experimental error.

2.4. Results

Figure 2 shows a typical result, with water depth plotted against the discharge rate. The expected increase in depth with flow rate can be seen as well as a distinct variation between the probes (gauges). The results of the individual probes were averaged before further analysis.

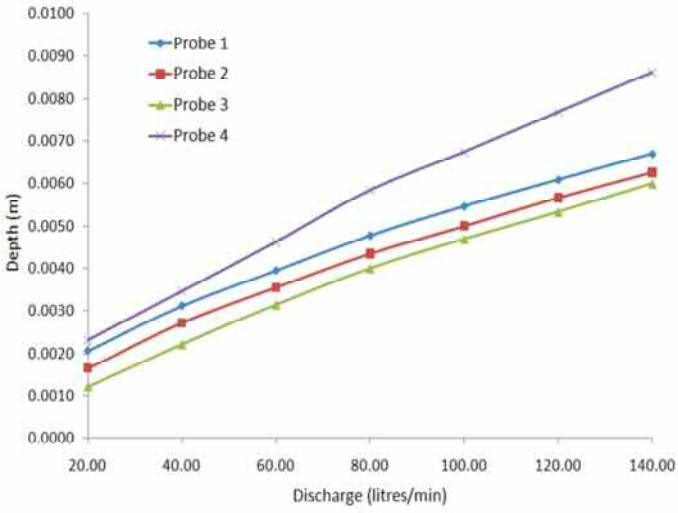

Figure 2 – Water depth against discharge rate for one of the tests

The objective of the measurements was to calibrate Equation 6 to the road surfaces in the study. However, in the experimental set up used, the flow rate of water reaching the top of the test sample under steady state conditions includes the effects of rainfall intensity (I) and upstream drainage length (L). As these effects cannot be differentiated, Equation 6 was revised by combining L and I:

$$d = k\,T^{w}\,(LI)^{y}\,S^{z} \qquad \text{Equation 7}$$

This was manipulated into a linear relationship by taking natural logarithms:

$$\ln(d) = \ln(k) + w\ln(T) + y\ln(LI) + z\ln(S) \qquad \text{Equation 8}$$

The values of k, w, y and z were determined by multiple linear regression of the data, resulting in the formula:

$$d = 5.9\times10^{-4}\,T^{0.087}\,(LI)^{0.59}\,S^{-0.33} \qquad \text{Equation 9}$$

The standard error associated with these parameter values ranged from 1% for the constant term, to approximately 4% for the exponents of the slope and LI terms, up to 6% for the exponent of the texture depth. The values of the exponents are consistent with the previous work apart from for the texture, where these results indicate a more pronounced impact of the texture depth on the water depth than has been reported before [4-7]. Figure 3 compares the experimental data for each surface with the model given by Equation 9. In each case the average water depth measured in the flume is plotted as filled points in blue, red and green for 0.5 %, 2 % and 6 % slopes, respectively, and the corresponding model values are shown as continuous lines in the same colour convention.

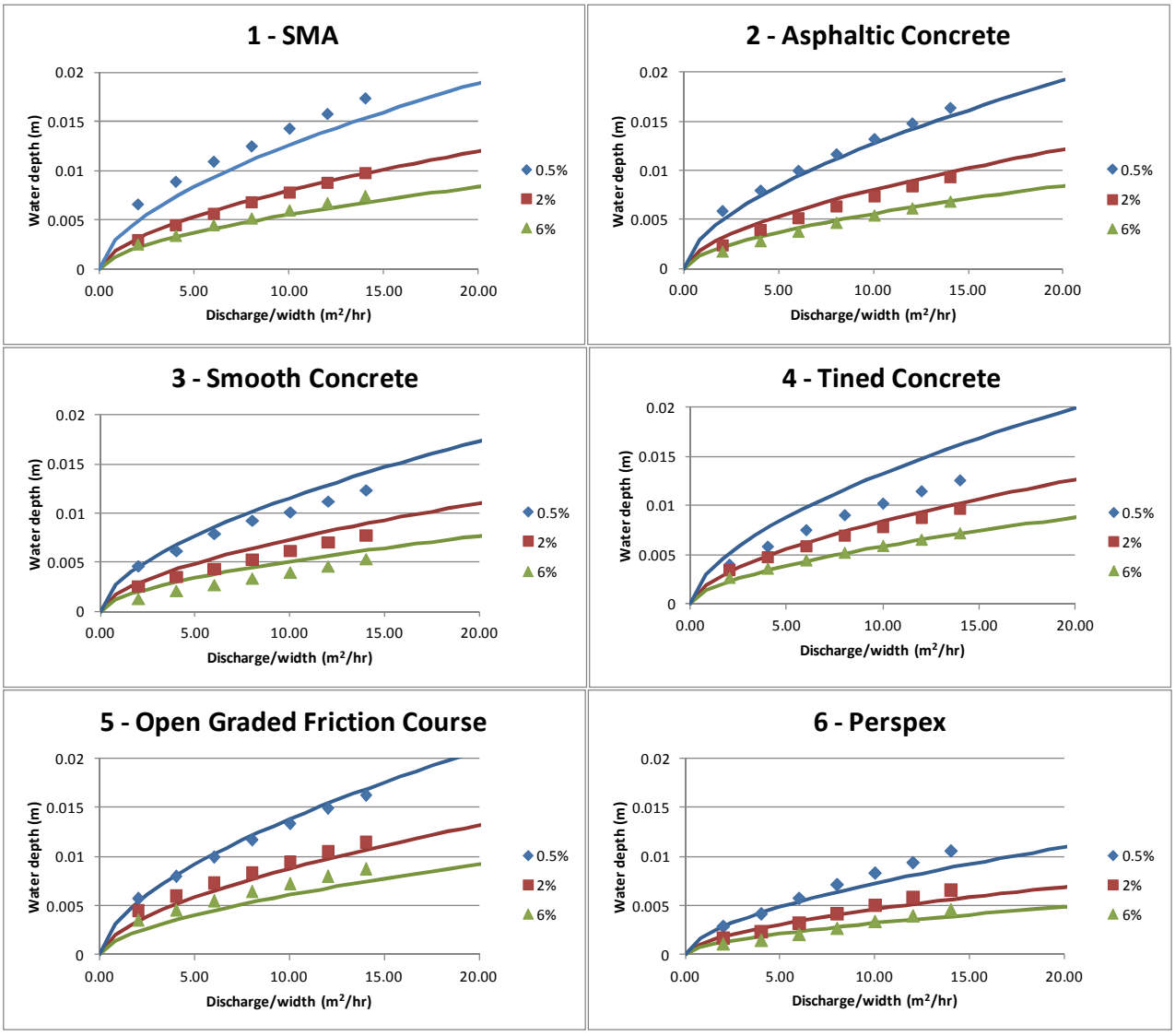

Figure 3 – Comparison of model to the experimental data for different surfaces and slopes

As expected, the steeper slopes result in lower depths of water. Surfaces with higher texture generate higher water depths, presumably because additional turbulence reduces

the flow rate of water, allowing a greater depth to build up. The depths of water in this experiment are much higher than the amount of water generally expected on the carriageway and so the assumption that the model can be reliably interpolated between the lowest water depths and the zero intercept is a limitation of the current work.

Figure 3 shows Equation 9 generally provides a good description of the experimental data although there are discrepancies for some of the data series, particularly the lowest slope. Equation 9 overestimates the water depth for the tined concrete and, to a lesser extent, the smooth concrete. Conversely, water depth is underestimated for the SMA and the Perspex. Of these discrepancies, the most pronounced difference is for the tined concrete; the experimental data for tined concrete are rather similar to the smooth concrete, suggesting the water flow is dominated by the smooth texture between the tines at low slopes, rather than by the presence of the tines and the greater texture they impart. With this exception, Equation 9 is judged to provide a good representation of the water depth as a function of discharge rate and slope.

3. DEVELOPMENT OF A SPLASH / SPRAY CFD MODEL

3.1. Introduction

This section describes the development of a computational fluid dynamic (CFD) model to investigate how this water is converted into splash / spray and gives preliminary results using this model. Much of the approach presented in this section is based on the findings of the Lawrence Livermore National Laboratories Heavy Vehicle Aerodynamics Project [8].

3.2. Geometry Build and Meshing

In the user perception studies carried out in this project [9], participants were asked to rate their reactions to a series of video clips taken from within a vehicle either following or passing a truck in wet conditions. The responses showed that a greater degree of nuisance (inferred from higher ratings for obstruction, concentration and risk, and lower ratings for confidence and control) was experienced for the following manoeuvre as compared with passing (overtaking). Also, a greater degree of nuisance was found for the dump truck compared with an articulated truck and when the second vehicle was a sedan compared with a SUV. These observations determined the basis of the CFD model, which was created for a typical sedan car following the GMC dump truck used in the user study.

The CFD model was created using a combination of photographs and reference measurements. Figure 4 shows the side view of the dump truck and the 3D solid model constructed. Working from photographs will inevitably introduce a number of inaccuracies and, in addition, smaller features such as wing mirrors, exhaust pipes and door handles were deliberately ignored because they would require a large number of cells to resolve them properly in the CFD model, adding perhaps an order of magnitude to the computational effort required. However, the solid model still preserves the bulk aerodynamic features of the body shell and the underside of the truck.

The solid model was subtracted from a rectangular volume constructed around it, leaving a void and this volume, the region in which fluid flow can take place, is meshed by being filled with cells. The cells are largely tetrahedral, with smaller cells used close to the truck to resolve detail and in regions where large velocity and pressure gradients might be expected. Viewing the volume mesh is unhelpful so Figure 5(a) and (b) shows the surface mesh in the vicinity of the rear and front wheels. The total mesh comprises 4.2 million

cells. This 3D model uses the GAMBIT CAD and meshing software, which is part of the ANSYS-FLUENT (hereafter referred to as Fluent) software suite.

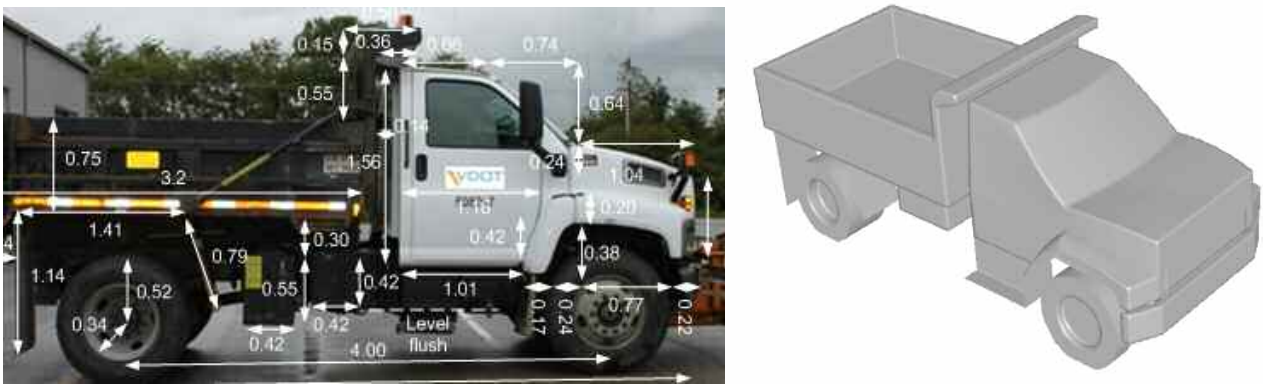

Figure 4 – Digitised photograph (left) and solid model (right) of the dump truck

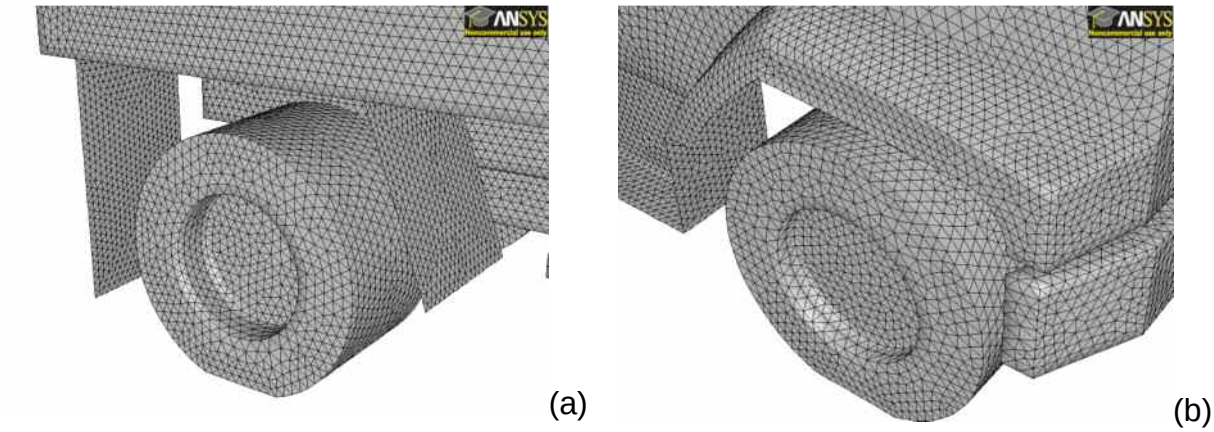

(a) (b)

Figure 5 – The surface mesh on (a) the rear and (b) front wheels

3.3. Set-up

3.3.1. Material Properties

Since incompressible flow was being modelled, the two important material properties for the air were its density, 1.225 kg/m^3, and dynamic viscosity, 1.79×10^{-5} Pa s.

3.3.2. Boundary Conditions

In the CFD model, the truck is held stationary and air enters the meshed domain at one end, passes around the truck and leaves via the other end. This frame of reference corresponds to that of an observer in the driver's seat as opposed to an external observer watching the vehicle go past. At the inlet, the air speed normal to the inlet is fixed at a value which corresponds to the speed of the truck, i.e. if the truck is travelling at 45 mph, the air speed is 20.1 m/s. Since the vehicle is travelling into still air, the turbulence intensity is set to 1% and the turbulence length scale to 1 m (Section 3.3.3). At the outlet, the relative pressure was set to 0.0 Pa. This does not correspond to a perfect vacuum, but rather is relative to atmospheric pressure. At this boundary, the air can leave unhindered.

The ground was modelled as a wall with a translational velocity aligned with and equal to the air velocity. Similarly, the wheels of the truck are rotated at a rate that is appropriate for the speed of the truck. For the 45 mph case, and a wheel diameter 0.5025 m, this equates to one revolution of the wheel every 0.1571 s, which means that the angular velocity of the wheel is 39.99 rad/s. The remaining boundaries – the sides and top of the domain – were modelled using symmetry boundary conditions. At these boundaries, the

normal derivatives of the field variables are zero. Such boundary conditions are often used to model distant boundaries in these situations. Indeed, this is one difference between the virtual and the real wind tunnel, which does have side walls and a roof.

3.3.3. Turbulence Model

The Reynolds number, Re, of the flow for the 45 mph case is 3.4×10^6, which means the flow is highly turbulent*. There are a variety of turbulence models available in Fluent, but here the RNG k-ε model was chosen because of its success in a previous project [10]. The simulation had to be run as unsteady because a steady-state solution would not converge due to the inherent unsteadiness of the wake behind the vehicle. Values of the field variables that are presented are therefore time-averages from a point where the simulation had reached a statistically stationary state.

3.3.4. Discrete Phase Model

The Discrete Phase Model (DPM) in Fluent is a Lagrangian particle tracking model, suitable for this application because the volume loading of the spray is small except in the region immediately next to the wheels [8]. The motion is described by:

$$m_d \frac{d\mathbf{u}_d}{dt} = \mathbf{F}_d + m_d\mathbf{g} \qquad \text{Equation 10}$$

where m_d is the mass of the droplet, $\mathbf{u}_d$ is the velocity of the droplet, $\mathbf{g}$ is the acceleration due to gravity and $\mathbf{F}_d$ is the aerodynamic drag

$$\mathbf{F}_d = \frac{1}{2} C_d \rho A_d |\mathbf{u} - \mathbf{u}_d|(\mathbf{u} - \mathbf{u}_d) \qquad \text{Equation 11}$$

where $\mathbf{u}$ is the air velocity, ρ is the air density, C_d is the drag coefficient and A_d is the area of the droplet presented to the flow. The drag coefficient is for a spherical droplet and is typically a complex function of the Reynolds number, based on the particle diameter, d.

The density of the droplets was set to 1000 kg m^{-3}. A range of droplet diameters were chosen, 100, 200, 500 and 1000 μm, which spanned the range in previous work [8]. There are a number of fates for the droplets once they are in flight:

- They can be trapped on a wall and thereby removed from the simulation
- They can reflect from a wall, the angle governed by restitution coefficients
- They can escape from the domain via the outlet.

In addition to the trajectory of the droplets being governed by Equation 10, the turbulence model imposes a random walk on the overall flight path, the magnitude of which is related to the turbulence level at the given point in space.

4. MODELLING OF SPLASH / SPRAY MECHANISMS

4.1. Approach

In the CFD process, water droplets are released into the air flow model, after which the trajectory of these particles is predicted within the turbulent air stream around the truck. An overall model for splash and spray will be developed from an understanding of the quantity of water arriving at a location likely to give rise to user nuisance under different starting conditions (i.e. different truck speeds and water depths).

* The Reynolds number was based on the vehicle speed and the width of the truck (2.5 m).

Research by Weir et al. [11] established four primary mechanisms by which the tire displaces the water in its path: bow wave, side wave, tread pickup and capillary adhesion. Figure 6 shows the approximate trajectory expected for water droplets following each mechanism. The following sections describe how the starting positions and velocities of water droplets have been determined to represent these different mechanisms. Water droplets are released from each of the two single front tires and two dual rear tires (Table 2 gives their sizes). The mesh of the tires defines the surfaces from which the water droplets are released, as shown in Figure 7. In practice, water droplets impacting other surfaces will result in other "sources" of spray. However, this effect has initially been neglected.

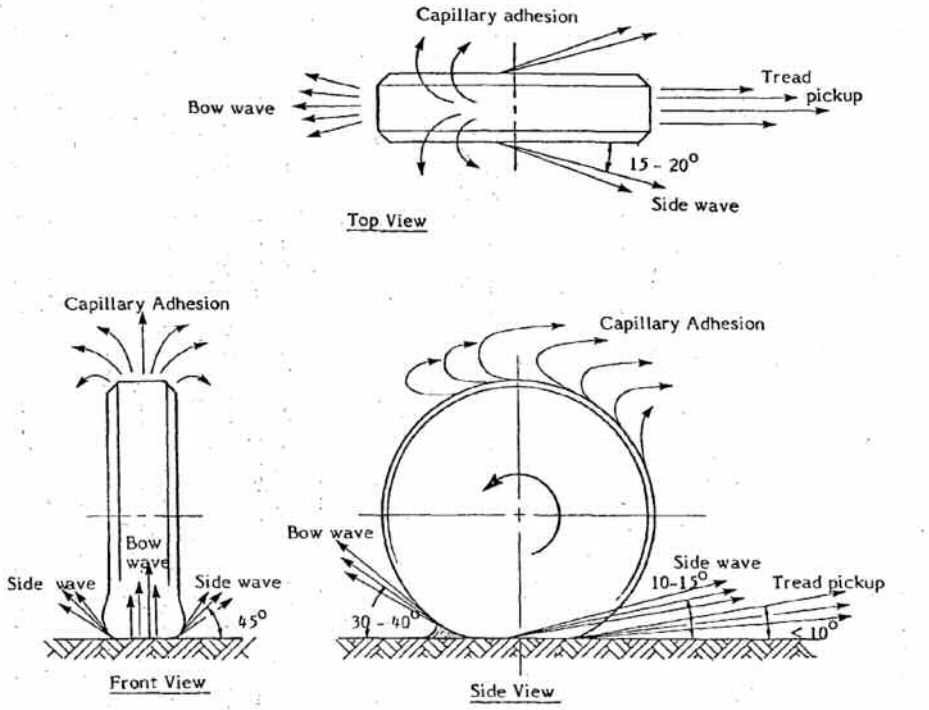

Figure 6 – Mechanisms for splash reproduced from Weir [11]

Table 2 – Tire geometry

	Tread width (mm)	Radius (mm)	Tread depth (mm)
Front wheel	280	502	10
Rear wheel	560	502	10

4.2. Capillary adhesion

Assuming it is not hydroplaning, the tire will remove the bulk of the water on the road such that only a small depth of water remains in the contact area between the tire and the road. A proportion of this amount of water will be attracted to the tire by surface tension at the contact interface and later will detach from the tire surface by the centripetal force due to the wheel rotation, giving rise to the mechanism of capillary action.

In the CFD frame of reference the truck is stationary and the ground is moving at speed V in the direction of the negative x axis. In Figure 8, this corresponds to the frame of reference (X,Y,Z) being attached to the truck and, in this frame, the tire is rotating with an angular velocity of ω. The initial tangential velocity at a point M on tire tread (surface S_{CA} in Figure 7) is determined as follows:

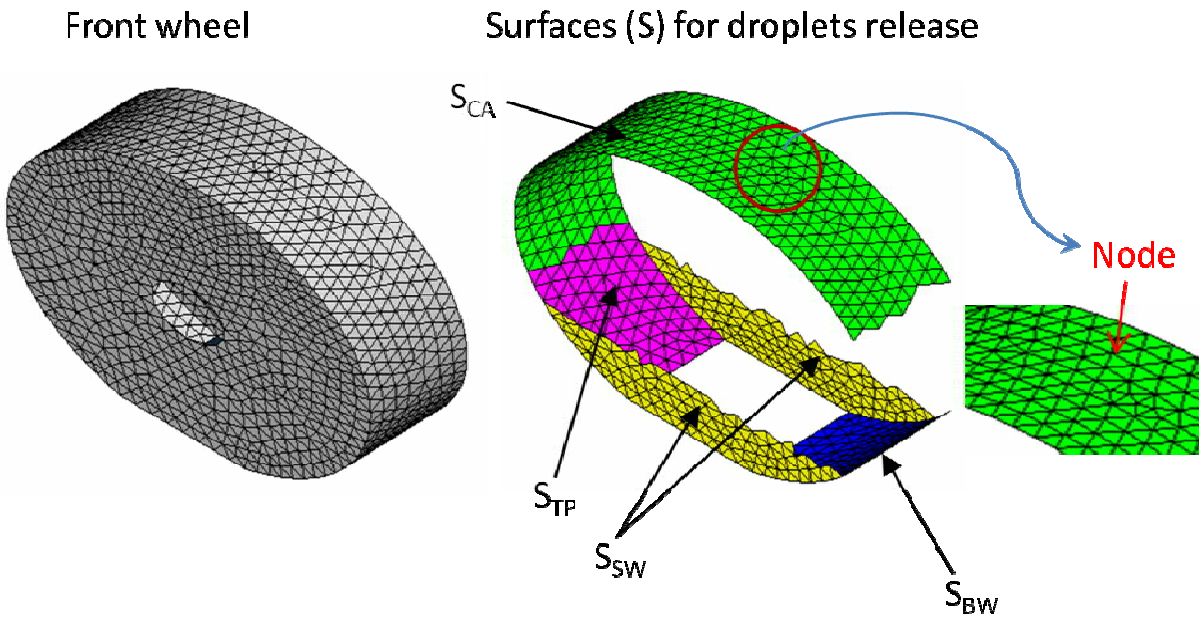

Figure 7 – Surfaces from which the water droplets are released to simulate the different mechanisms: S_{CA} capillary adhesion; S_{TP} tread pickup; S_{BW} bow wave; S_{SW} side wave

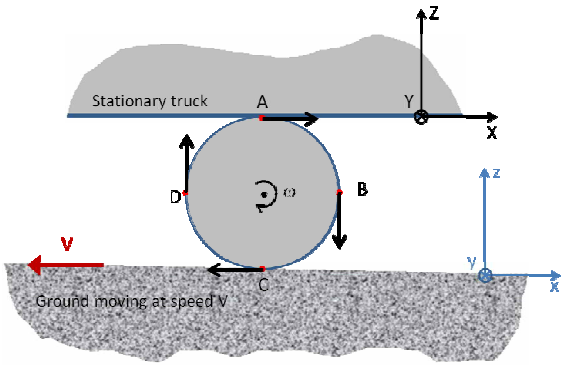

Figure 8 – Kinematic condition of a tire in the CFD model

1) Let u, w be the coordinate of point M with respect to the tire's centre, where u//x, w//z.

2) Calculate $A = u / \sqrt{(u^2 + w^2)}$ and $B = w / \sqrt{(u^2 + w^2)}$

3) Calculate $A = \arccos\left(u / \sqrt{(u^2 + w^2)}\right) * 180 / \pi$ and $B = \arcsin\left(w / \sqrt{(u^2 + w^2)}\right) * 180 / \pi$

4) Calculate the angular directions l_x, and l_z of the initial velocity v_M as:

Calculate l_x :

If $B \geq 0$ then $l_x = A$

If $(A < 0 \text{ and } B < 0)$ then $l_x = a - 2b$

If $(A > 0 \text{ and } B < 0)$ then $l_x = 360 - a$

Calculate l_z :

$l_z = l_x - 90$

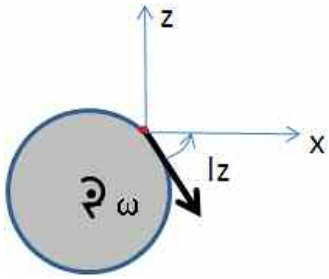

5) Calculate the initial velocity v_M as:

$$v_x = \omega\sqrt{\left(u^2 + w^2\right)} * \cos\left(l_z * \pi/180\right)$$
$$v_y = 0$$
$$v_z = \omega\sqrt{\left(u^2 + w^2\right)} * \sin\left(l_z * \pi/180\right)$$

Equation 12

4.3. Tread pickup

After capillary action, the tire displaces a volume of water within its tread. Figure 9 depicts the initial velocities associated with tread pickup from zone S_{TP} at an angle l=10°. The initial velocity $\vec{V}_{TP}$ is coplanar with the plane xz and it is assumed the magnitude of the velocity is the same as the truck speed, V. The components of the initial velocity are:

$$v_x = -V\cos(\pi l/180)$$
$$v_y = 0$$
$$v_z = V\sin(\pi l/180)$$

Equation 13

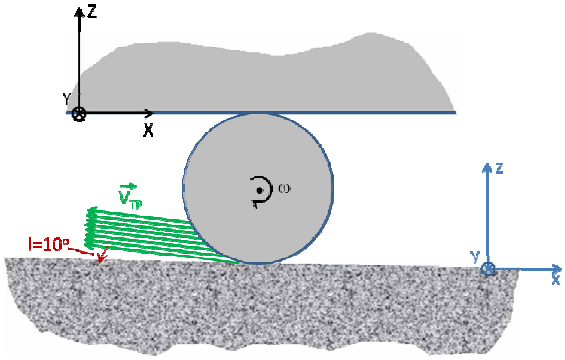

Figure 9 – Representation of the initial velocity for droplet released from zone S_{TP}

4.4. Bow wave

Any remaining water for which there is no capacity either underneath the tire contact area or within the tire tread must be displaced either to the front of the tire or to the side, causing the bow wave and side wave, respectively. In the frame of reference attached to the truck, the body of water on the road will impact the tire at a speed equal to the truck speed. It is assumed that the bow wave emerges at an angle l with respect to the x axis, (Figure 10) with speed V_{BW}, defined as:

$$\vec{V}_{BW} = \varsigma V$$

Equation 14

where V is the truck speed and ζ is a constant

The case of V_{BW}=V corresponds to an elastic impact. The effects of varying ζ between 0.1 and 0.75 are shown in Figure 11. Higher values of zeta are associated with the bow wave having a trajectory above the level of the bonnet. The cases with ζ=0.1 and ζ=0.2 were judged to be more realistic and a value of ζ=0.2 has been used.

Assuming that the bow wave occurs in the plane (x,z), the components of the initial velocity $\vec{V}_{BW}$ are:

$$v_x = \varsigma V\cos(\pi l/180)$$
$$v_y = 0$$
$$v_z = \varsigma V\sin(\pi l/180)$$

Equation 15

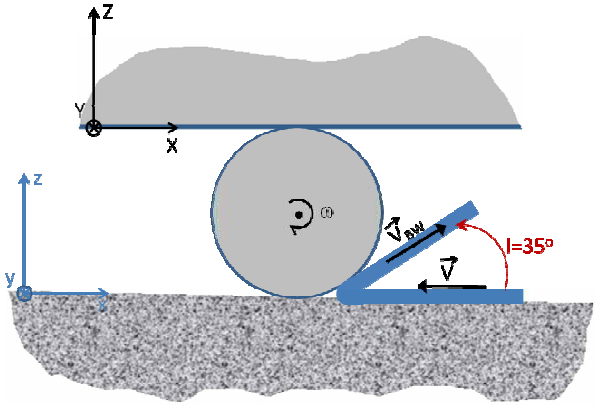

Figure 10 – Representation of the initial velocity for droplet released from zone S_{BW}

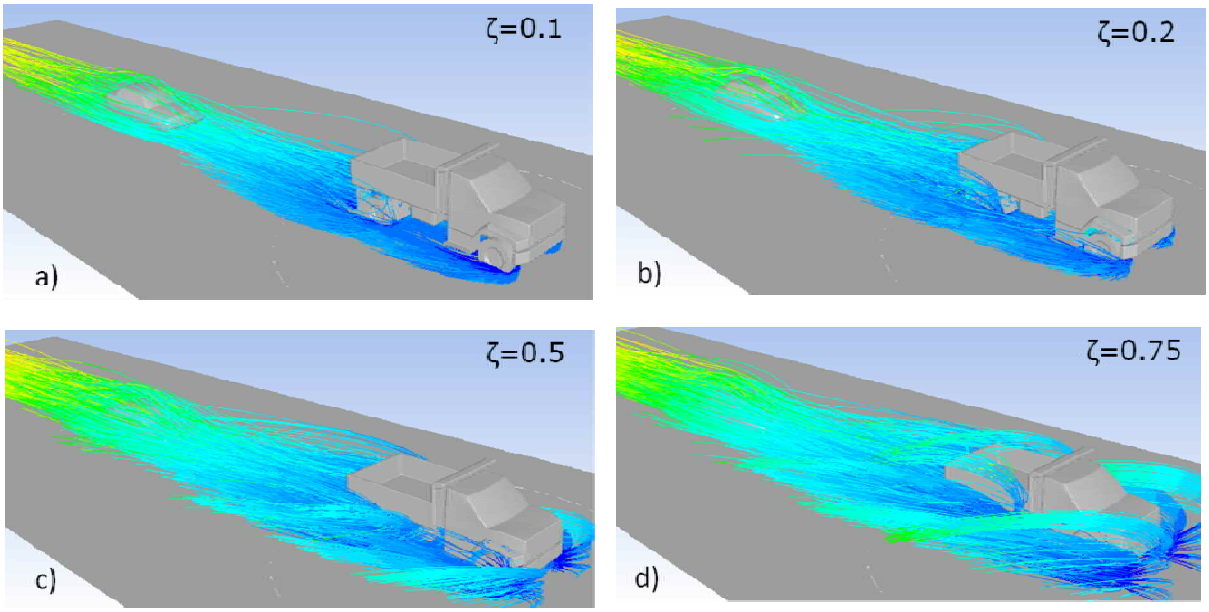

Figure 11 – Effect of the parameter ζ on the shape of the bow wave, V= 45mph

4.5. Side wave

The initial velocity of the side wave is defined by the vector $\vec{V}_{SW}$ depicted in Figure 12. It is assumed that its horizontal component, v_x, is equal to the speed of the vehicle, hence using the configuration of Figure 13, the magnitude of the initial velocity V_{SW} is derived as:

$$V_{sw} = V\sqrt{\left(1+\tan^2(\pi l/180)+\tan^2(\pi n/180)\right)} \qquad \text{Equation 16}$$

and the vector components v_x, v_y and v_z are derived as:

$$v_x = -V$$
$$v_y = \pm V\tan(\pi n/180) \qquad \text{Equation 17}$$
$$v_z = V\tan(\pi l/180)$$

From Figure 6, the range of the angle l is defined to be between of 10° and 15°, and the range of the angle n is between of 15° and 20°. For this work, angles l and n are varied according to the position of the node within the zone S_{sw}, to provide a dispersion of the water droplets away from the tire.

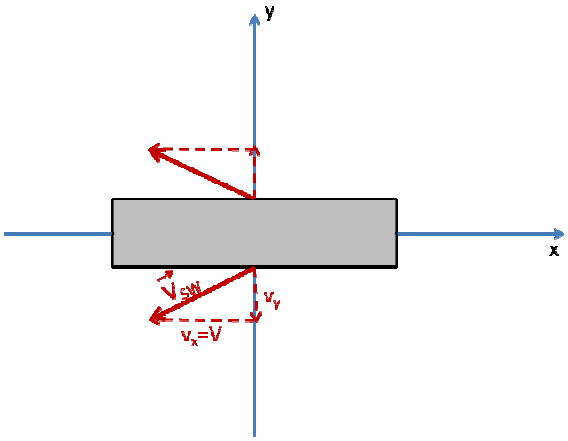

Figure 12 – Representation of the initial velocity for droplet released from zone S_{SW}

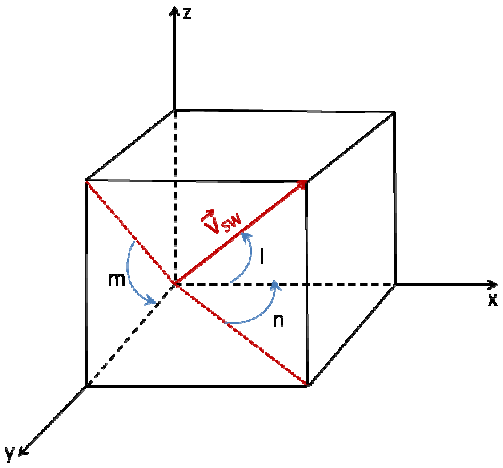

Figure 13 – Resolution of the side wave directions in a Cartesian coordinates

5. INITIAL CFD RESULTS

The immediate trajectories of the droplets after being released are shown in Figure 14. Each coloured line represents the trajectory of an individual droplet and the change of colour from blue, to light blue, to green, represents the trajectory of the droplet during successive time intervals. The trajectories are broadly consistent with Figure 6, confirming the velocity vectors have been correctly established in the injection file.

Figure 15 shows how the trajectories develop during the CFD modelling. Again, the differences between the mechanisms appear to be in line with expectations: capillary adhesion results in rather high trajectories that take a significant proportion of droplets directly onto the windscreen of the following vehicle. In contrast, trajectories arising from tread pick up remain closer to ground level and the particles ejected from the rear tires appear to fall quickly to ground level – the trajectories end just behind and to the side of the truck where they impact with the road surface. Of all the mechanisms, tread pickup appears to be the one that will result in least nuisance to the following car.

The bow wave particles begin by travelling forward and are rapidly displaced to the side of the vehicle by the airstream. These also tend to remain close to the ground. For the side wave the trajectories are higher, which may cause nuisance to a vehicle overtaking the truck but, within the present model, the car following the truck appears to be relatively unaffected by either the bow wave or side wave.

Combining the different mechanisms, it can be seen that the sensitivity to increasing vehicle speed appears to be convincing (Figure 16). However, modelling the effects of the combined mechanisms requires an estimate of the relative mass flow rates for each to estimate the overall level of nuisance to road users.

6. SUMMARY, CONCLUSIONS AND NEXT STEPS

The experimental work carried out in the flume has enabled a relationship for the water depth present on the road surface to be calibrated as a function of the road geometry, surface texture and rainfall intensity. Here, the road geometry is the upstream path length

and slope, itself being the result of the local crossfall and gradient, all of which can be determined from the geometry data provided by typical surface condition surveys.

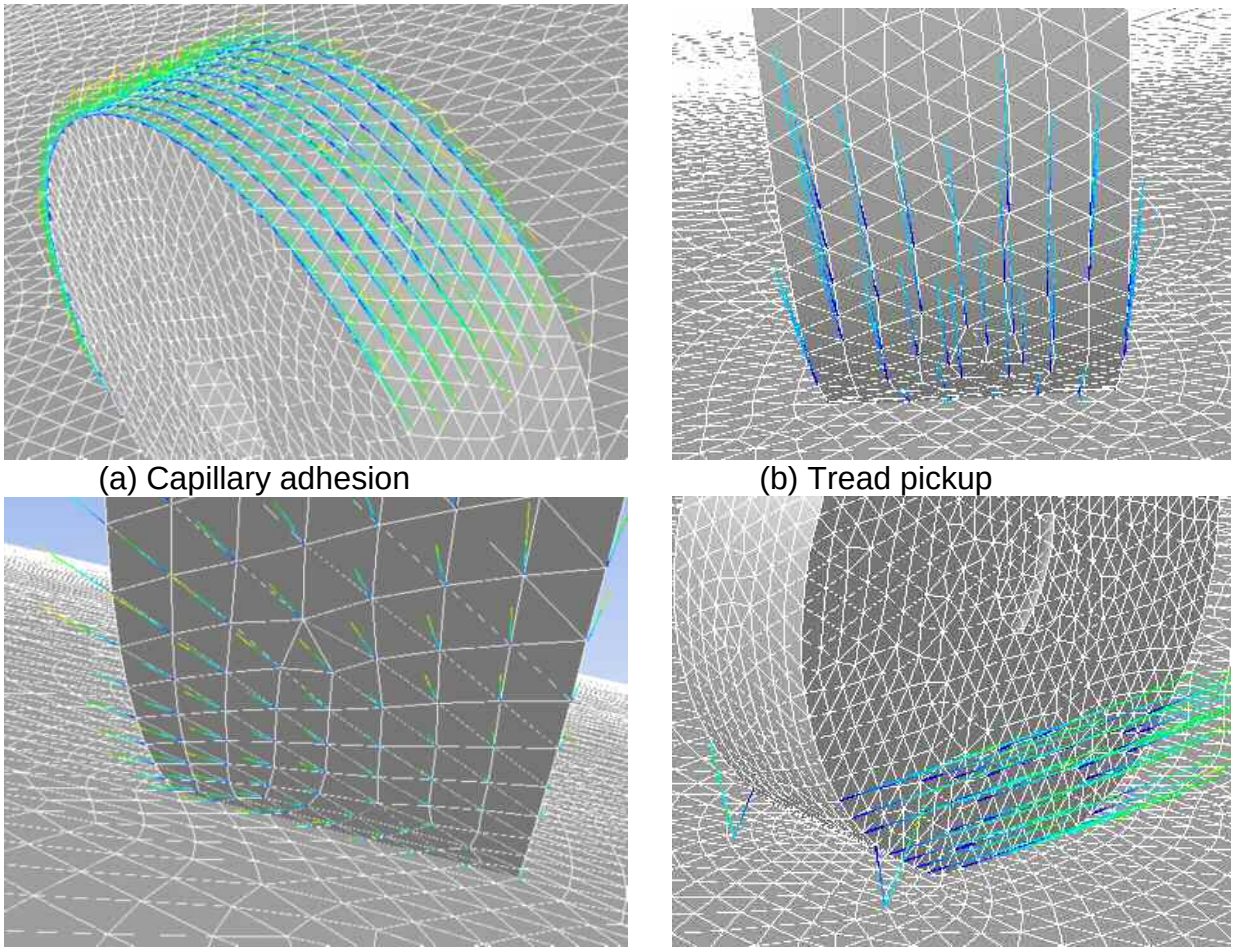

(a) Capillary adhesion (b) Tread pickup

(c) Bow wave (d) Side wave

Figure 14 – Simulation results – initial velocities for each zone, viewed from above, behind, in front of and to the side of the tire, respectively

A CFD model has been developed for the 4 major mechanisms believed to contribute to splash and spray in the case of a sedan car following a dump truck. The initial modelling suggests the nuisance caused to the driver of the following vehicle increases in the order capillary adhesion > bow wave > side wave > tread pickup. It appears that the side wave will be particularly problematic to vehicles overtaking the truck, although the different airflows in this case would require a different model to be created to verify this.

While capillary adhesion appears to be most likely to cause nuisance to a following vehicle, the mass flow rate of water associated with this mechanism is likely to be lower than for the other mechanisms. Estimating the relative magnitudes of these effects will be important to determine the overall nuisance, and this may also be affected by the presence of porous surfaces. This is planned in the next stage of the project.

It will also be necessary to quantify the overall degree of nuisance and this can readily be achieved by deriving metrics of the density of water droplets at key locations. In the user perception work carried out within this project [9], user ratings were found to correlate strongly with the degree of obscuration of a checkerboard carried on the back of the truck, therefore the volume of water being deposited on the windscreen or the volume of water contained in a volume at windscreen height in the space between the truck and the car are relevant measures that can readily be determined from the CFD output.

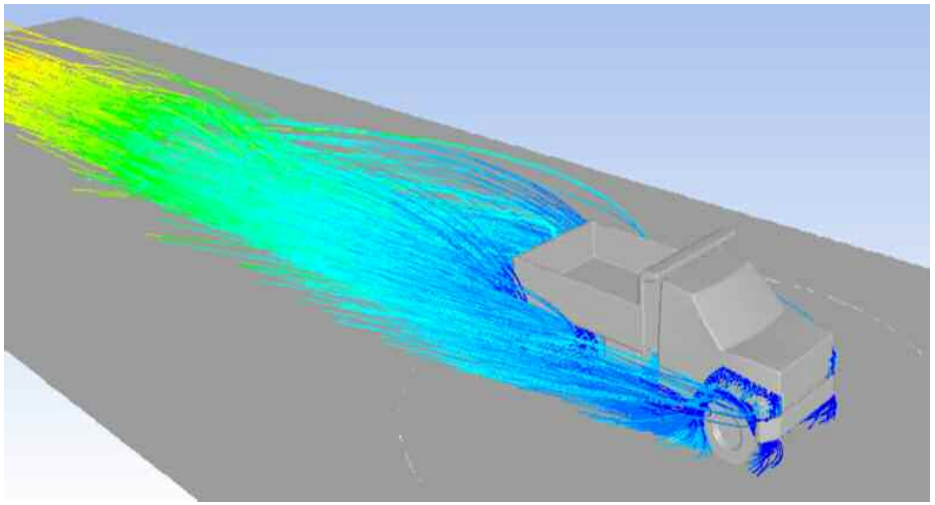

(a) Capillary adhesion

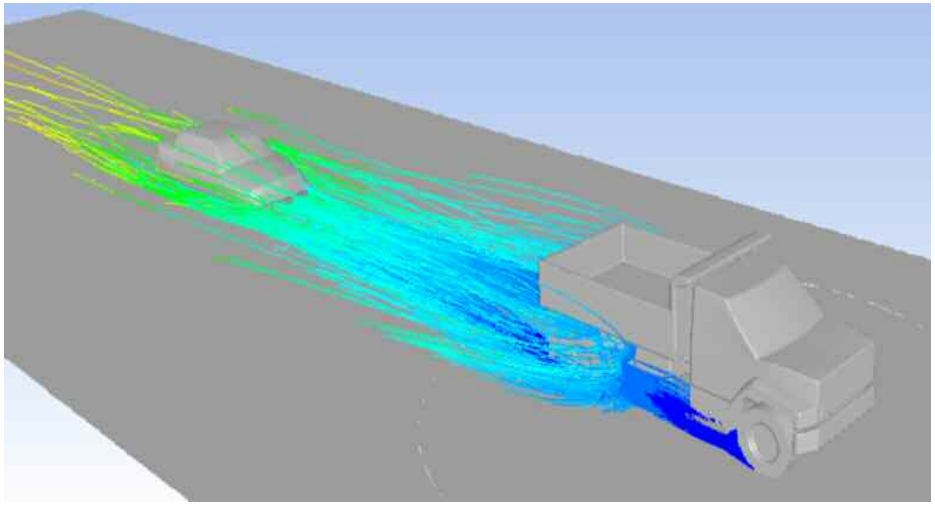

(b) Tread pickup

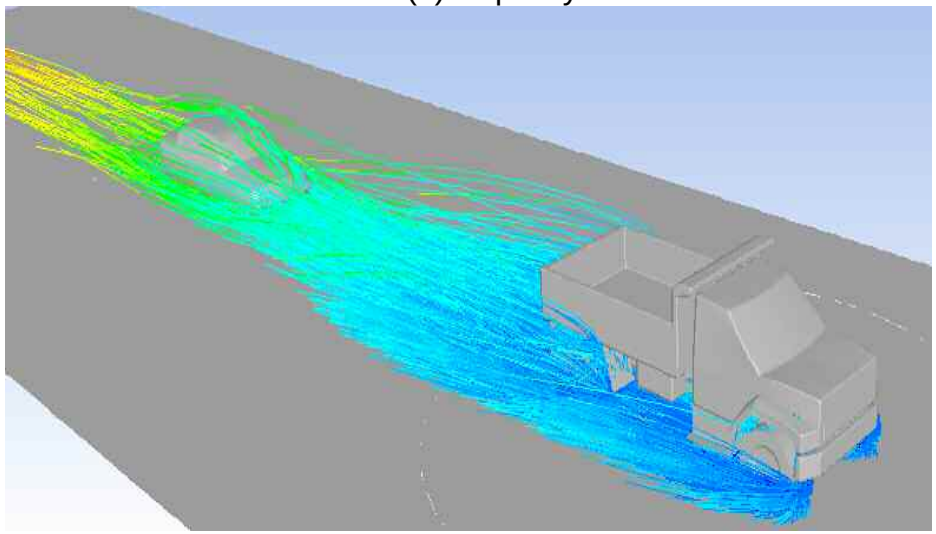

(c) Bow wave

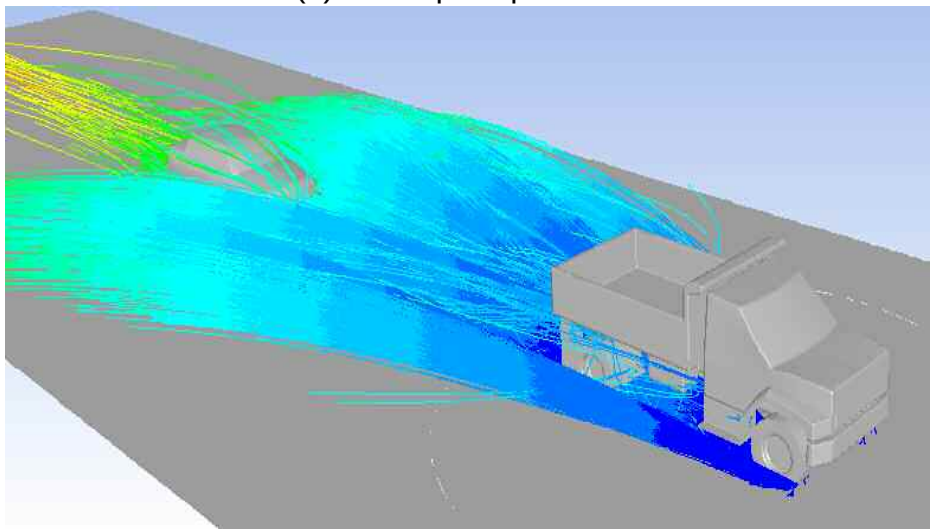

(d) Side wave

Figure 15 – Simulation results – droplet trajectories resulting from each mechanism

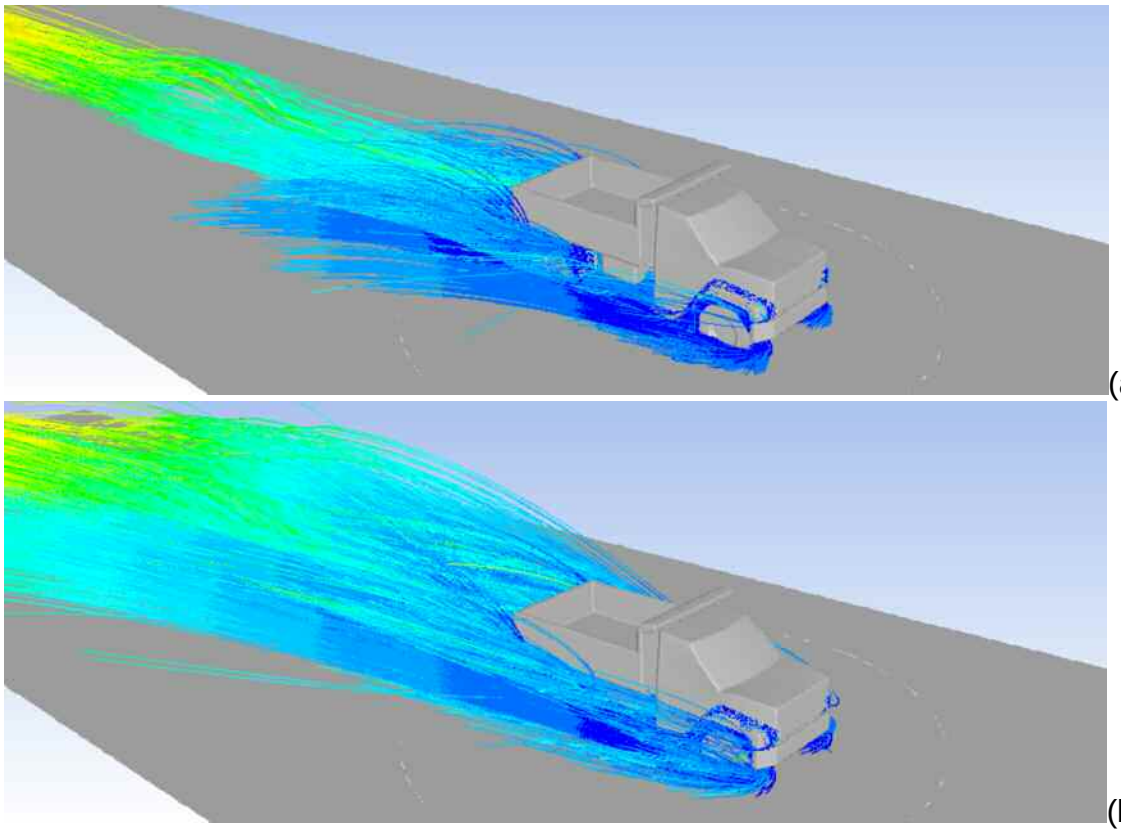

Figure 16 – Simulation results – sensitivity to speed: (a) 30 mph (b) 60 mph

Therefore, an overall nuisance model can be developed that determines the likelihood of certain water depths occurring given the road characteristics and local climate data, and how this is translated into user nuisance via the generation of splash and spray. This work is due to be completed during 2012.

REFERENCES

1. Tromp JPM (1985). Splash and spray by lorries. Report R-85-5. Institute for Road Safety Research SWOV, The Netherlands.
2. Knight I, Dodd M, Bowes D Donaldson W, Smith T, Neale M, Grover C and Couper G (2005). Integrated safety guards and spray suppression – final report. TRL report PPR075. TRL, Crowthorne, Berkshire, UK.
3. Resendez YA, Sandberg U, Rasmussen RO and Garber S (2007). Characterising the splash and spray potential of pavements. Synthesis report carried out for the U.S. Department of Transportation Federal Highway Administration.
4. Ross, N. F. and Russam, K. (1968). The depth of rain water on road surfaces. Wokingham: Road Research Laboratory.
5. Gallaway, B. M., Schiller, R. E., and Rose, J. G. (1971). The effects of rainfall intensity, pavement cross slope, surface texture and drainage length on pavement water depths. Texas: Texas Transportation Institute.
6. Roe, P. G., Hewitt, A. P., Parry, A. R., May, R. W., and Cheetham, R. J. (1997). Water depths on wide carriageways - a laboratory study. Crowthorne: Transport Research Foundation.
7. Anderson, D. A., Huebner, S. R., Reed, J. R., Warner, J. C., and Henry, J. J. (1998). Improved surface drainage of pavements. Pennsylvania: The Pennsylvania Transportation Institute.
8. Paschkewitz J (2006). Simulation of spray dispersion in a simplified heavy vehicle wake. Lawrence Livermore National Laboratory
9. Flintsch GW, Williams B, Gibbons R and Viner H (2012). Assessment of the Impact of Splash and Spray on Road Users - Controlled Experiment Results. Transportation Research Board paper 12-3684.
10. Sterling M, Quinn AD, Hargreaves DM, Sabbioni E, Tomasini G (2010). A comparison of different methods to evaluated the wind induced forces on a high sided lorry. *J. Wind Eng. Ind. Aero 98, 10-20.*
11. Weir DH, Strange JF and Heffleny RK (1978). Reduction of adverse aerodynamic effects of large trucks.